

Constraints on the Ratio between Tropical Land and Ocean Precipitation Derived from a Conceptual Water Balance Model

LUCA SCHMIDT^{a,b} AND CATHY HOHENEGGER^a

^a *Max Planck Institute for Meteorology, Hamburg, Germany*

^b *International Max Planck Research School on Earth System Modelling, Hamburg, Germany*

(Manuscript received 18 August 2022, in final form 27 January 2023, accepted 17 March 2023)

ABSTRACT: Which processes control the mean amounts of precipitation received by tropical land and ocean? Do large-scale constraints exist on the ratio between the two? We address these questions using a conceptual box model based on water balance equations. With empirical but physically motivated parameterizations of the water balance components, we construct a set of coupled differential equations that describe the dynamical behavior of the water vapor content over land and ocean as well as the land's soil moisture content. For a closed model configuration with one ocean and one land box, we compute equilibrium solutions across the parameter space and analyze their sensitivity to parameter choices. The precipitation ratio χ , defined as the ratio between mean land and ocean precipitation rates, quantifies the land–sea precipitation contrast. We find that χ is bounded between zero and one as long as the presence of land does not affect the relationship between water vapor path and precipitation. However, for the tested parameter values, 95% of the obtained χ values are even larger than 0.75. The sensitivity analysis reveals that χ is primarily controlled by the efficiency of atmospheric moisture transport rather than by land surface parameters. We further investigate under which conditions precipitation enhancement over land ($\chi > 1$) would be possible. An open model configuration with an island between two ocean boxes and nonzero external advection into the domain can yield χ values larger than one, but only for a small subset of parameter choices, characterized by small land fractions and a sufficiently large moisture influx through the windward boundary.

KEYWORDS: Tropics; Rainfall; Advection; Atmosphere–land interaction; Water budget/balance

1. Introduction

All water that evaporates from Earth's land and ocean surfaces must eventually return to the surface as precipitation. This water mass balance also holds approximately in the tropics. But which physical processes or parameters of the system determine how much it rains over land versus over ocean? A useful quantity in the context of the large-scale tropical land–sea contrast of precipitation is the precipitation ratio χ , defined as the ratio of spatiotemporally averaged precipitation rates over tropical land and ocean. Modern observations make it easy to quantify χ but do not explain its value. Similarly, the complexity of sophisticated climate models limits clear process understanding and, apart from that, these models frequently fail to reproduce observed precipitation patterns (Fiedler et al. 2020) as well as the right land–sea contrast of precipitation (Hohenegger and Stevens 2022). It is therefore the aim of this study to provide theoretical understanding of the large-scale constraints on χ that arise from the water mass balance, as well as the sensitivity of χ to different physical processes and properties of the system. To this end, we consider a simple box model with a small number of free parameters such as land fraction or land surface characteristics. As such, this model is not meant to realistically describe the real tropics. Rather, it helps us understand fundamental relationships and identify relevant mechanisms for which more sophisticated investigations are needed.

Hohenegger and Stevens (2022) is the first study to compute χ from different observation products and to use a conceptual rainbelt model to interpret the obtained values with respect to the role of land for precipitating convection. Accounting for the tropical land–ocean geometry as well as width, intensity, and latitudinal position of the rainbelt, the χ values from observations, ranging between 0.9 and 1.04, could only be explained if the nature of the surface, being land or ocean, affects the rainbelt characteristics. In other words, the presence of land affects the way it rains. The authors concluded that land receives more precipitation than what is expected from the mere geometry of the tropical landmasses. Similar to Hohenegger and Stevens (2022), we study the physical controls on χ and draw indirect conclusions about the relationship between precipitation and the underlying surface. However, we take a different, independent approach which is agnostic about the land geometry and spatial structure of precipitation. With our box model consisting of one ocean and one land domain, we examine the theoretical upper and lower bounds of χ that arise solely from the condition of water balance.

While the large-scale land–sea contrast of precipitation remains poorly investigated, much work using box models and water balance equations has been directed at the question of how the presence of land impacts local rainfall. Unlike the ocean, land can dry out and thereby significantly reduce its evaporative moisture flux. The degree to which precipitation hinges on local evapotranspiration determines how susceptible precipitation is to changes in soil moisture conditions and therefore to the underlying surface. With their one-dimensional land–atmosphere model based on water balance equations,

Corresponding author: Luca Schmidt, luca.schmidt@mpimet.mpg.de

DOI: 10.1175/JHM-D-22-0162.1

© 2023 American Meteorological Society. For information regarding reuse of this content and general copyright information, consult the [AMS Copyright Policy](#) (www.ametsoc.org/PUBSReuseLicenses).

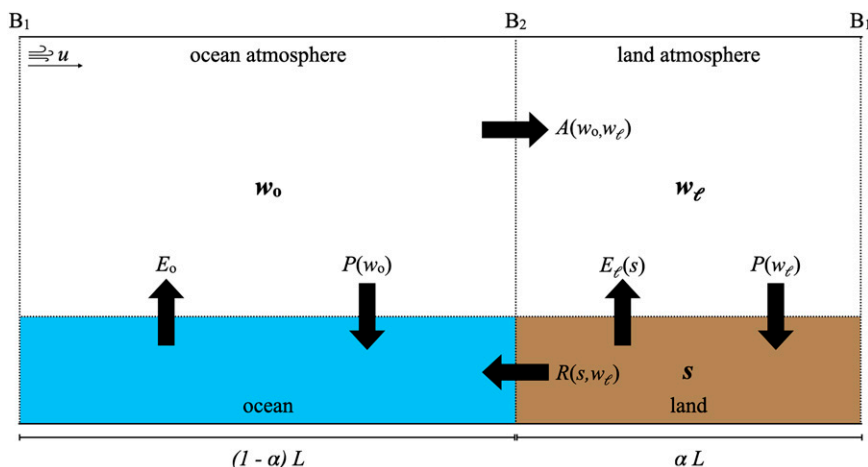


FIG. 1. Model sketch of the land–ocean–atmosphere system with periodic boundary conditions. The length of the boxes is determined by the total domain length L (km) and land fraction α . Black arrows represent the box-averaged moisture fluxes (mm day^{-1}) between the four model boxes. An exception is the advective net exchange A between the atmospheres that represents the total net amount of transferred moisture ($\text{mm}^2 \text{day}^{-1}$) and translates to different mean fluxes, A_o and A_l (mm day^{-1}), out of or into these boxes due to the different box lengths. The atmospheric moisture transport is driven by a constant horizontal background wind speed u . All fluxes other than ocean evaporation E_o , which is a constant model parameter, are functions of the relative soil moisture saturation s , or water vapor paths of land and ocean atmospheres, w_l and w_o , respectively.

Budyko and Drozdov (1953) lay the foundation for quantifying land–atmosphere coupling by computing moisture recycling ratios for different continental regions. The recycling ratio measures the share of precipitation inside a region that is derived from locally evaporated moisture, as opposed to advected moisture from outside the region. Important subsequent studies that computed recycling ratios include Brubaker et al. (1993), Eltahir and Bras (1994), and van der Ent et al. (2010). While the obtained contributions from local evapotranspiration to rainfall varied between 10% and 90%, depending on the selected region and employed method, all studies agreed on that soil moisture availability leaves an imprint on the terrestrial precipitation signal.

Such moisture recycling studies as well as the hydrological studies by Rodriguez-Iturbe et al. (1991) and Entekhabi et al. (1992), who used a land box model based on water balance equations to understand the controls on soil moisture variability, inspired our approach and helped us design our conceptual model. However, these studies only consider terrestrial precipitation and prescribe the contributions from advected moisture. Advected moisture itself, which likely plays a role in setting χ , is not part of their solution. We therefore couple our land and ocean domains through advection and runoff, and allow for an interactive exchange of moisture between them. As a consequence, land and ocean precipitation rates and, hence, χ arise as part of the solution to our model equations.

2. Model description

To understand the controlling factors and constraints for the land–sea precipitation contrast, we propose a box model

as sketched in Fig. 1. The model consists of an ocean subdomain denoted by subscript o and a land subdomain denoted by l whose sizes are determined by the full domain length L and land fraction α . Each subdomain contains a ground box at the bottom (ocean or land) and an atmospheric box above. The vertical extent of the atmospheric boxes is chosen as the height over which water vapor is transported and stored. Similarly, the vertical depth of the land box is given by the hydrologically active soil depth z_r . In the horizontal direction, the model has periodic boundary conditions, which makes it a closed system that conserves water. Such a closed model (CM) is suitable to describe the entire Earth or, if net moisture exchange with the extratropics is negligible, the tropics. In section 6, we discuss an open model (OM) version which allows for nonzero net advection from outside the model domain.

a. Water balance equations

To formulate the underlying water balance equations, we express all moisture fluxes between the boxes as functions of the system's moisture state. For atmospheric boxes, the moisture state is given by the mean water vapor path w (mm), and for the land box by the unitless mean relative soil moisture saturation s . Since the ocean does not dry out, it does not require a moisture variable. Hence, the full information on the moisture state of the land–ocean–atmosphere system at any moment in time t is given by the set of state variables $\{w_o(t), w_l(t), s(t)\}$.

The time evolution of the state variables is expressed by coupled water balance equations in which the water fluxes

represent moisture sinks and sources (see, e.g., [Brubaker et al. 1991](#)):

$$\frac{ds}{dt} = \frac{1}{nz_r} [P(w_\ell) - R(s, w_\ell) - E_\ell(s)], \quad (1)$$

$$\frac{dw_\ell}{dt} = E_\ell(s) - P(w_\ell) + A_\ell(w_\ell, w_o), \quad (2)$$

$$\frac{dw_o}{dt} = E_o - P(w_o) + A_o(w_\ell, w_o). \quad (3)$$

Note that the time dependence of s , w_ℓ , and w_o is implicit in Eqs. (1)–(3). The relevant fluxes, indicated by the black arrows in [Fig. 1](#), are precipitation P , land evapotranspiration E_ℓ , ocean evaporation E_o , soil runoff R , and atmospheric advection A . The advection terms A_ℓ and A_o in Eqs. (2) and (3) represent the box-mean net advection rates into the land and ocean atmosphere, respectively, and are positive for net moisture import and negative for net moisture export. In a closed system, the domain-mean advection vanishes, i.e., $\alpha A_\ell + (1 - \alpha)A_o = 0$. All fluxes are given as spatial mean flux rates in millimeters per day (mm day^{-1}). The product of dimensionless soil porosity n and hydrologically active soil depth z_r (mm) is a model parameter.

b. Empirical relationships for water fluxes

To solve the water balance equations (1)–(3), we need expressions for the water fluxes. While the conservation of water is a fundamental condition, there are no simple fundamental laws governing the moisture exchange between the model boxes. Instead, we use empirical relationships, as has been done, for instance, by [Rodríguez-Iturbe et al. \(1991\)](#). As in their study, we express runoff as the fraction R_f of precipitation that does not infiltrate into the soil,

$$R(s, w_\ell) = R_f(s)P(w_\ell), \quad (4)$$

with

$$R_f(s) = \epsilon s^r, \quad (5)$$

and the two dimensionless parameters ϵ and r . Equation (5) tells us that runoff intensifies as the soil moistens. Runoff water is returned to the ocean but has no effect on the ocean’s moisture properties.

For precipitation, [Rodríguez-Iturbe et al. \(1991\)](#) followed the approach of [Budyko and Drozdov \(1953\)](#) which assumes that the advected part of land precipitation is known. This is not a desirable assumption in our case where the focus is on the factors controlling the land-to-ocean precipitation ratio. We want a free interaction between the two subdomains and therefore choose to parameterize precipitation as a function of w , as established by [Bretherton et al. \(2004\)](#) based on observations,

$$P(w) = \exp \left[a \left(\frac{w}{w_{\text{sat}}} - b \right) \right]. \quad (6)$$

Equation (6) introduces two dimensionless parameters a and b , and the saturated water vapor path w_{sat} (mm). Whether the

exact shape of the $P(w)$ relationship, here set by the choice of a , b , and w_{sat} , is identical over land and ocean is still under debate. While [Schiro et al. \(2016\)](#) and [Schiro et al. \(2020\)](#) reported only slight differences in the $P(w)$ relationship between tropical land and ocean regions, a similar study by [Ahmed and Schumacher \(2017\)](#) found that land precipitation increases more strongly at lower water vapor path values than ocean precipitation, and that it exhibits a diurnal cycle, presumably due to stronger surface heating and orographic effects. Our hypothesis here is that the processes which turn water vapor into precipitation depend only on the atmospheric vapor concentration and not on the underlying surface. Hence, we use Eq. (6) with the same parameter values over land and ocean. Indirectly, by comparing our model results to observed values of χ , we can return to this debate and assess whether the nature of the underlying surface affects the $P(w)$ relationship (see [section 6a](#)).

The qualitative dependence of evapotranspiration on soil moisture saturation is long known (see, e.g., [Budyko 1956](#)). [Seneviratne et al. \(2010\)](#) present a schematic, where E_ℓ is close to zero for soil moisture values below the permanent wilting point, $s < s_{\text{pwp}}$, increases approximately linearly in a transition range between the permanent wilting point and a critical value close to the field capacity, $s_{\text{pwp}} < s < s_{\text{fc}}$, and reaches a plateau for higher s values, $s > s_{\text{fc}}$, where evapotranspiration is nearly constant at its potential rate e_p . For computational convenience, we parameterize evapotranspiration by the following smooth function which has the qualitative properties described above,

$$E_\ell(s) = \frac{e_p}{2} \left\{ \tanh \left[10 \left(s - \frac{s_{\text{pwp}} + s_{\text{fc}}}{2} \right) \right] + 1 \right\}. \quad (7)$$

Unlike land, the ocean is always fully saturated, and we assume the resulting ocean evaporation rate to be a constant model parameter $E_o = e_o$.

It remains to find expressions for the mean net advection rates for the land and ocean atmospheres, hereafter just land/ocean advection. The total net advection into a given box is the difference between the moisture entering and leaving the box per unit time, which is computed from the windward and leeward boundary water vapor paths (in mm) times mean horizontal wind speed u (in mm day^{-1}), respectively. Because we assume one uniform w across each atmospheric box, the wind transports the moisture amount $w_o u$ from ocean to land and $w_\ell u$ from land to ocean, resulting in a net exchange of $A(w_o, w_\ell) = \pm(w_o - w_\ell)u$. For the advection rates per unit length (mm day^{-1}), this gives

$$A_\ell(w_o, w_\ell) = \frac{(w_o - w_\ell)u}{\alpha L} = \frac{(w_o - w_\ell)}{\alpha} \tau \quad (8)$$

for land advection and

$$A_o(w_o, w_\ell) = -\frac{(w_o - w_\ell)u}{(1 - \alpha)L} = -\frac{(w_o - w_\ell)}{(1 - \alpha)} \tau, \quad (9)$$

for ocean advection, with α being the land fraction and L the total domain length (see [Fig. 1](#)). On the right-hand sides of Eqs. (8) and (9), we introduced the atmospheric transport

TABLE 1. Free parameters for the closed model simulations with uniform random sampling of parameter values.

Parameter	Minimum	Maximum	Range choice motivated by
s_{pwp}	0.15	0.55	Hagemann and Stacke (2015)
e_p (mm day ⁻¹)	4.0	6.0	Entekhabi et al. (1992)
nz_r (mm)	50.0	120.0	Entekhabi et al. (1992)
e_o (mm day ⁻¹)	2.5	3.5	Kumar et al. (2017), Zhang and McPhaden (1995)
ϵ	0.9	1.1	Rodriguez-Iturbe et al. (1991), Entekhabi et al. (1992)
r	2	6	Rodriguez-Iturbe et al. (1991), Entekhabi et al. (1992)
a	11.4	15.6	Bretherton et al. (2004)
b	0.5	0.6	Bretherton et al. (2004)
w_{sat} (mm)	65.0	80.0	Bretherton et al. (2004)
α	0.0	1.0	Full possible range
$\tau = u/L$ (day ⁻¹)	0.00216	0.864	Plausible ranges for L and u

parameter $\tau = u/L$ (day⁻¹). Its inverse value τ^{-1} represents a characteristic time scale for atmospheric transport. Similar concepts were used by Brubaker et al. (1991), Sobel and Bellon (2009), and Lintner et al. (2013) to model advection. In a closed system, this formulation of advection with a constant, unidirectional wind field results in a downgradient net transport of atmospheric moisture. In our case this net transport carries moisture from a moister ocean atmosphere to a drier land atmosphere which is not always the case in reality (Brubaker et al. 1991).

c. Parameter ranges

We want to constrain χ for our system in equilibrium and test its sensitivity to parameter choices. To do that, we need to define plausible ranges for all free model parameters, thereby constructing our search space. The chosen ranges are summarized in Table 1.

The ranges for s_{pwp} and s_{fc} are taken from data for different soil types presented in Hagemann and Stacke (2015), where we discard the extreme cases of pure sand and peat. After converting the provided volumetric data to relative soil moisture saturation values, s_{pwp} ranges between 0.15 and 0.55. We notice the fairly consistent relationship, $s_{\text{fc}} = s_{\text{pwp}} + 0.3$, and use it to reduce the number of free model parameters by one. Entekhabi et al. (1992) provide values for e_p , nz_r , r , and ϵ for both a semihumid and a semiarid climate. We take the values from these two climates as limits for the respective parameter ranges and vary e_p between 4 and 6 mm day⁻¹ and nz_r between 50 and 120 mm. Entekhabi et al. (1992) set $r = 6$ for both cases but we let the runoff exponent range between 2 and 6, motivated by Rodriguez-Iturbe et al. (1991) who used $r = 2$ in an illustrative example. Since both studies agree on $\epsilon = 1$, we vary this parameter only slightly between 0.9 and 1.1. Note that ϵ values larger than one could lead to unphysical solutions where runoff exceeds precipitation. Such unphysical cases must be excluded from the analysis, but it turns out they never occur. The precipitation parameters are taken from Bretherton et al. (2004) (where our b is called r). We use their fitting parameter values for monthly and daily data as bounds for a and b . Bretherton et al. (2004) also give a typical value, $w_{\text{sat}} = 72$ mm, for regions of tropical convection and we deem it appropriate to vary w_{sat} between 65 and 80 mm. Ocean evaporation can be constrained from observations. For

instance, Kumar et al. (2017) found the mean evaporation from tropical ocean surfaces to range between 2.5 and 2.8 mm day⁻¹, while an earlier study by Zhang and McPhaden (1995) indicates higher values of about 3.5 mm day⁻¹. Based on these findings, we let e_o range between 2.5 and 3.5 mm day⁻¹. This range also encompasses 3 mm day⁻¹—the mean value of precipitation over both tropical land and ocean. Last, τ is constrained by computing the smallest and largest value of u/L , respectively, where we assume plausible wind speeds in the lower troposphere between 1 and 10 m s⁻¹, and let the domain length vary between 1000 and 40 000 km, the upper limit corresponding to Earth's equatorial circumference. Thus, we obtain a range for τ between about 0.002 and 0.864 day⁻¹.

d. Model assumptions

The simplicity of the proposed model owes to a number of assumptions, some of which are important to be made explicit. Foremost, we assume that each model box has well-mixed physical properties so that all interactions are adequately described in terms of spatial mean quantities. Second, we determine the system's moisture state by water balance equations only, ignoring the potential effects of energy balance considerations such as the influence of a diurnal cycle. Energetic conditions are kept constant and only enter indirectly through the values of energy-dependent parameters such as e_o or w_{sat} . Third, we prescribe a background wind speed with only a horizontal and constant component. Last, and more importantly, we assume that the functional relationship between precipitation and water vapor path from Eq. (6) holds over both land and ocean with the same choice of parameter values. By comparing the range of obtained χ values from our simple model to known values from the real world, we will discuss in section 6a what we can conclude about the potential processes that control the land–sea precipitation contrast in the real world.

3. Methodology

Here, we present the different analysis methods that are employed to evaluate the model behavior and to assess the sensitivity of the land-to-ocean precipitation ratio to variations of the parameter values. The land-to-ocean precipitation ratio is defined as

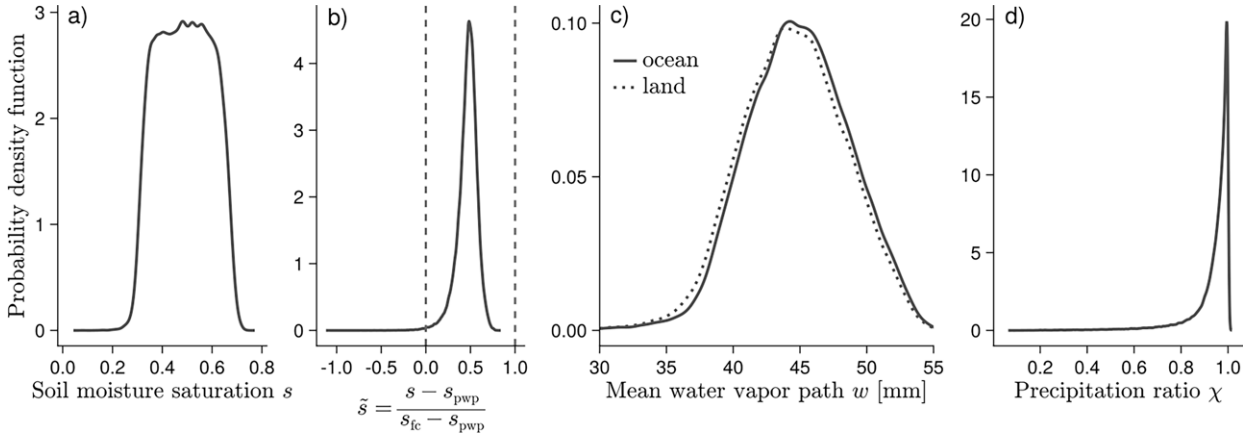


FIG. 2. (a) Smoothed probability density functions of equilibrium soil moisture values; (b) rescaled soil moisture values with vertical lines denoting the permanent wilting point and field capacity which mark the beginning and end of the transition regime of E_t , respectively; (c) water vapor path of the land and ocean atmospheres; and (d) values of χ . For improved visibility of water vapor path differences between land and ocean in (c), the distribution’s tails toward very dry and very moist states, representing less than 0.23% of the simulations, are not shown.

$$\chi = \frac{P_\ell}{P_o} = \frac{P(w_\ell)}{P(w_o)}. \tag{10}$$

The equilibrium solution to the model equations (1)–(3) has to be found numerically. We use the DynamicalSystems.jl library from Datsaris (2018) to find all roots of the model equations which represent stable fixed points of the system. Adopting an agnostic view on the plausibility of different combinations of parameter values from the ranges in Table 1, we perform 100 000 model simulations for randomly chosen points in the 11-dimensional parameter space, each yielding a corresponding equilibrium state and resulting fluxes. Scatterplots are used to analyze the sensitivity of χ to the different model parameters.

A suitable measure for the dependence of some quantity Q on a parameter p , which accounts for the possibility of a non-linear and nonmonotonic relationship between Q and p , is their mutual information $MI(Q, p)$. Mutual information quantifies how much the knowledge of p reduces the uncertainty about Q . The mutual information of p and Q is computed as

$$MI(Q, p) = H(Q) + H(p) - H(Q, p), \tag{11}$$

where $H(Q)$, $H(p)$, and $H(Q, p)$ are the Shannon entropies of Q and p values, and of their joint distribution, respectively (Shannon 1948). To ascribe the probability distributions required for the computation of the Shannon entropies, we use amplitude binning with 10 equally sized bins for both Q and p .

To put the mutual information value into perspective, we follow the approach from Datsaris and Parlitz (2022, p. 106), and assess whether the obtained $MI(Q, p)$ is significantly different from the null hypothesis of independent Q and p . From the mutual information values of 1000 shuffled surrogates of Q and p , we compute a probability distribution of MI values for the uncorrelated case and define $MI_{\text{uncorr},3\sigma}(Q, p)$ as the value that deviates by three standard deviations σ

from the mean of this distribution. The mutual information index,

$$I_{MI}(Q, p) = \frac{MI(Q, p)}{MI_{\text{uncorr},3\sigma}(Q, p)}, \tag{12}$$

can then be used to assess how the actual mutual information $MI(Q, p)$ compares to the value one would expect if Q and p were unrelated. We choose $I_{MI} = 1$ to be the threshold for a significant sensitivity of Q to p , with higher $I_{MI}(Q, p)$ values reflecting a higher sensitivity. In this work, we compute the mutual information index $I_{MI}(\chi, p_i)$ for all free model parameters p_i in order to rank and compare the sensitivity of χ to these different parameters.

4. Basic model behavior and implications for χ

We performed 100 000 closed model simulations with different parameter choices, each yielding exactly one stable equilibrium solution to the model equations (1)–(3). The output of these simulations is henceforth referred to as “CM data.” In this section, we analyze these data with the aim of determining the range of possible equilibrium values of χ . Note that the presented results proved to be qualitatively robust to variations in the number of performed simulations.

We begin by characterizing the obtained equilibrium states and associated moisture fluxes. Figure 2 illustrates the characteristics of possible equilibria through probability density functions (PDF) of equilibrium soil moisture values in Figs. 2a and 2b, and water vapor path values for land and ocean atmospheres in Fig. 2c. In Fig. 2b, s is rescaled to $\tilde{s} = (s - s_{\text{pwp}})/(s_{\text{fc}} - s_{\text{pwp}})$ such that the equilibrium values are located relative to the different regimes of evapotranspiration discussed in section 2b. The regimes are separated by the permanent wilting point and field capacity, which are each indicated by a dashed vertical line. The bulk of all simulations equilibrates to intermediate soil moisture values

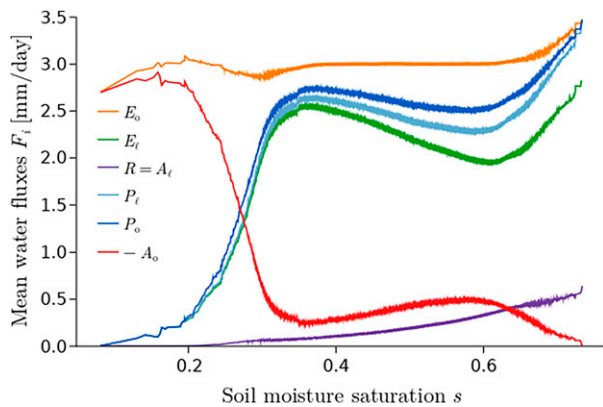


FIG. 3. Moving average over different fluxes vs soil moisture saturation computed from the CM data. For the moving average, we sort the data by s and compute the average flux rates within a window of 20 000 simulations symmetrically centered around each value of s . Toward the limits of s , the window's size is reduced in order to retain its symmetric positioning.

between $s = 0.25$ and 0.75 with a sharp peak in the center part of the E_l -transition regime around $\bar{s} = 0.5$. Only a few simulations (0.38%) equilibrate to a very dry state with soil moisture values below the permanent wilting point. We discuss such dry states in section 5b. Similarly, the atmospheres mostly equilibrate to intermediate w_o and w_l values between 40 and 50 mm (see Fig. 2c), well below w_{sat} . As a matter of comparison, a value of $w = 48$ mm is often employed to distinguish the moist deep tropics with deep convection from the dry subtropics (Masunaga and Mapes 2020). For better visibility of the differences between w_o and w_l in Fig. 2, we cut the tails of very dry and very moist atmospheric states which represent less than 0.23% of all simulations. Figure 2c shows that land and ocean generally equilibrate to similar atmospheric moisture values but that the land is slightly drier than the ocean.

Figure 3 shows moving averages of the equilibrium fluxes from all simulations as functions of the equilibrium soil moisture saturation. Note that the ocean advection rate A_o has negative values in all solutions and is therefore multiplied by -1 to simplify the comparison of its magnitude with other fluxes. Figure 3 contains the entire CM data so that the emerging behavior of the fluxes is a result of a plethora of different parameter choices with soil moisture values being the result, not the driver. Therefore, one should not confuse the plotted curves with the well-defined parameterizations of the water fluxes as functions of s for a fixed set of parameter values.

The purple line in Fig. 3 represents both land advection and runoff. That a net moisture transport from ocean to land balances the land's loss of moisture through runoff is a long-known characteristic of the equilibrated hydrological cycle, see, e.g., Horton (1943) or Peixoto and Oort (1983). We can use this fact to derive an upper bound of χ : According to the advection equations (8) and (9), net moisture transport from ocean to land requires the ocean atmosphere to be moister than the land atmosphere, $w_o > w_l$. Since the same, monotonically increasing function $P(w)$ from Eq. (6) is used

over land and ocean, $P(w_o)$ is necessarily larger than $P(w_l)$. In other words, it rains more strongly over ocean than over land. This is confirmed by Fig. 3 where the dark blue curve for P_o always lies above the light blue curve for P_l . Hence, in our water balance model, an upper bound on χ exists, this upper bound being $\chi = 1$. That χ is bounded by one is also apparent from Fig. 2d, which shows the PDF of χ values. While the lower bound is essentially zero, corresponding to cases where land precipitation vanishes, low values of χ are rare and 82.9% of all parameter combinations yield values larger than 0.9, thereby falling into the range obtained by Hohenegger and Stevens (2022) from observations.

The shapes of the lines in Fig. 3 indicate that three soil moisture–precipitation regimes can be distinguished: For low equilibrium soil moisture values up to $s \approx 0.36$, runoff and land advection are negligible and P_l nearly equals E_l which rises sharply with s . In an intermediate soil moisture regime, $0.36 \leq s \leq 0.61$, P_l decreases due to a decline of E_l . However, the precipitation decrease is slightly damped by a steadily growing contribution of moisture from land advection (purple line). Last, above $s \approx 0.61$, precipitation increases again as the evapotranspiration trend reverses and advection keeps intensifying.

The equilibrium fluxes in Fig. 3 exhibit a number of surprising behaviors: Why is there hardly any rain over ocean when the soil is dry? Why does advection out of the ocean atmosphere (red line) tend to decline with increasing s while advection into the land atmosphere (purple line) increases monotonically? And why does evapotranspiration decline in the intermediate regime while soil moisture increases? To answer these questions, we need a better understanding of how the different model parameter choices and combinations thereof influence the attained equilibrium states and fluxes. The sensitivity of χ to variations in the model parameters and explanations for the seemingly unphysical behaviors in Fig. 3 are the topic of the next section.

5. Parameter sensitivity of χ

Having established that χ is bounded between zero and one in our water balance model, we want to better understand the controls of different parameters on the attained equilibrium value. To this end, we quantify the sensitivity of χ to each individual model parameter by the mutual information index $I_{\text{MI}}(\chi, p_i)$ defined in Eq. (12). A comparison of the results for all model parameters p_i is provided in Fig. 4. The atmospheric transport parameter τ is by far the most influential parameter, followed by the soil parameters permanent wilting point s_{pwp} and runoff exponent r , and the land fraction α . Some of the remaining parameters also have I_{MI} values above or close to the significance threshold (dashed line) but we do not discuss them in detail due to their rather small contributions to the overall sensitivity. Note that the relative importance of different parameters for χ is not caused or reflected by the relative magnitude of the moisture fluxes associated with these parameters. For instance, the fact that two important parameters, τ and α , both appear in the advection term does not imply that advection is the strongest flux, in fact it never is as illustrated

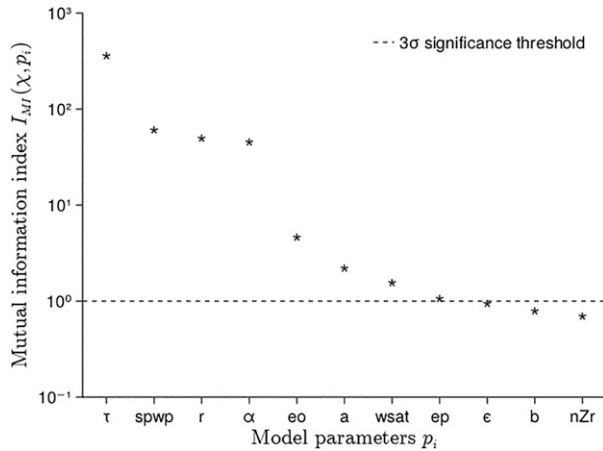


FIG. 4. Relative sensitivity of χ to the different model parameters p_i measured by the mutual information index I_{MI} . Values larger than $I_{MI} = 1$ (dashed line) lie above the significance threshold.

in Fig. 3. The importance of τ and α is also not related to the fact that advection is the only linear flux parameterization. A similar sensitivity analysis for a model version with linear expressions for all moisture fluxes (not shown) still identified τ and α as the parameters with the strongest control on χ .

Figure 5 shows scatterplots of χ versus the four most influential model parameters. The respective mean of χ values along each parameter is shown by a white line and the spread around this mean is generated by variations in all other model parameters. In this section, we discuss the physical mechanisms by which these most important parameters influence χ .

a. Atmospheric transport parameter τ

The relationship between χ and τ in Fig. 5a is strongly non-linear and leads to variations of the χ mean between 0.5 and 0.98, confirming the high sensitivity determined in the mutual information analysis. Physically, τ corresponds to the fraction of the domain length that moisture can travel horizontally in the atmosphere in one day. As such, it can be interpreted as the efficiency of atmospheric moisture transport or efficiency of horizontal mixing: The higher the value of τ , the more efficient the mixing, and the lower the moisture differences, $\Delta w = w_o - w_l$, between the two atmospheres. Since we link precipitation and atmospheric moisture through the same parameterization $P(w)$ over land and ocean, a small Δw implies similar precipitation rates over land and ocean and a χ value close to one. In contrast, inefficient mixing due to small values of τ can sustain larger moisture differences between land and ocean and leads to smaller values of χ . This theoretical control of τ on χ is confirmed in Fig. 5a where χ tends to be small for low values of τ and converges toward one as τ increases.

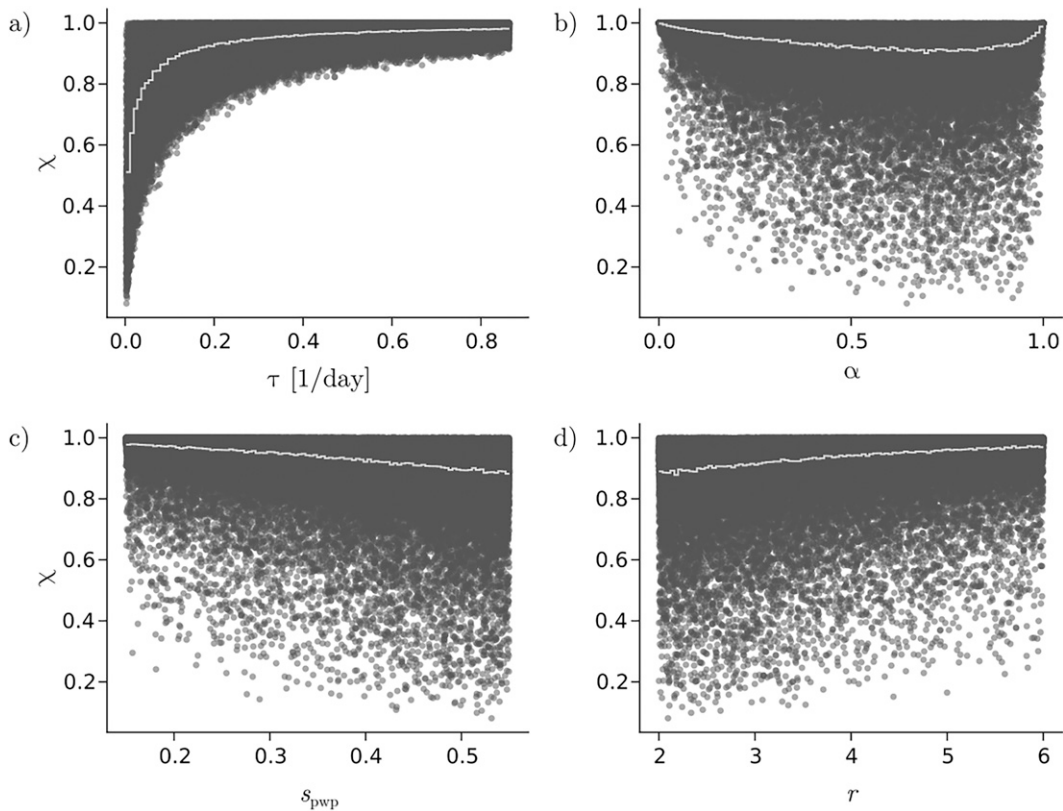


FIG. 5. Precipitation ratio χ vs atmospheric transport parameter τ , land fraction α , permanent wilting point s_{pwp} , and runoff exponent r . The white lines show χ mean values computed for 100 bins along the parameter axis.

The spread around the τ mean is reduced as τ increases, making τ a better predictor for χ , the larger its value. Figure 5a also suggests that τ has a strong control on the lower bound of the spread around the χ mean which increases with τ . In contrast, the upper bound of the spread, $\chi = 1$, seems independent of τ .

We can understand how τ influences the lower bound of the spread of χ values by returning to the advection equations (8) and (9), each of which can be rephrased as the product of Δw and an advection efficiency, namely, τ/α for land advection and $\tau/(1 - \alpha)$ for ocean advection. Only if both advection efficiencies are low, a large moisture difference and, hence, small χ can be sustained. The land fraction affects ocean and land advection efficiencies in opposite ways, suggesting a minimum of overall advection efficiency for intermediate α . If advection was the only process at play, this minimum would be located at $\alpha = 0.5$, and it would be left to τ to set the final value of the lowest possible advection efficiency, and thereby the smallest possible χ for that value of τ . In the following, we will see that the complexity of land–atmosphere interactions adds further parameter controls on the lower bound of χ and leads to an asymmetry in the relationship between χ and α such that the lowest χ value is found at a larger land fraction than $\alpha = 0.5$.

b. Land fraction α

Figure 5b illustrates how α impacts the value of χ . The χ mean varies between 0.91 and 1.0 on a u-shaped line between the extreme cases of an ocean-only, $\alpha = 0$, and land-only, $\alpha = 1$, scenario where in both cases χ is close to one. As for τ , the impact of land fraction changes on the value of χ is rooted in their control on the advection efficiencies, τ/α and $\tau/(1 - \alpha)$. The particular role of α is to differentiate between the efficiency of moisture export out of the ocean subdomain and the efficiency of moisture import into the land subdomain by setting the different areas over which the advected moisture gets distributed. If α is small, the imported moisture gets distributed over a small land size, making land advection efficient and the rate per unit area high. The reverse applies for a large land fraction. In either case, mixing between the two atmospheres is efficient and the smaller atmosphere adopts the moisture conditions of the larger one, resulting in a χ value close to one.

While the model cannot handle the exact endpoints of the α range, we can examine them in a thought experiment: imagine a domain fully covered by ocean. Water balance would require the ocean precipitation to balance ocean evaporation, $P_o = E_o$. If we now introduced an infinitesimal patch of land, some of the evaporated moisture would be advected into the tiny land atmosphere without significantly altering the moisture conditions over the vast ocean. Since τ/α is high, the atmospheric conditions over land would rapidly converge to those over the ocean. Hence, for such small α , the system is expected to behave as if the land did not exist. Atmospheric conditions would be overall moist with nearly the same land and ocean precipitation rates close to E_o , leading to a χ of one. At the other extreme, imagine a pure land domain but

with the assumption that runoff to some external reservoir remains possible. The runoff would continuously reduce the soil moisture saturation and with it evapotranspiration and precipitation until the trivial equilibrium solution $\{s = 0, w_\ell = 0\}$ is reached. Allowing for advection from an infinitesimal ocean would not change the picture much. With high efficiency $\tau/(1 - \alpha)$, almost the entire but nevertheless small amount of evaporated oceanic moisture would be exported to the land, leaving behind a fairly dry ocean atmosphere and hardly affecting the dry state of the large land atmosphere and soil. Hence, the system would behave as if the ocean did not exist with similarly low precipitation rates close to zero in both subdomains.

The transition between the ocean-only and land-only scenario is best understood by examining the individual rain rates P_o and P_ℓ over the range of α as shown in Fig. 6. The two extremes are connected by a regime of monotonic drying as the ocean surface—the only true source of moisture for the system’s hydrological cycle—shrinks. Although not shown, the overall reduction of available moisture as the land fraction increases also manifests itself in a soil moisture decrease. We can investigate the shapes of P_ℓ and P_o theoretically, assuming all parameters except α to be fixed. Expressions for the rain rates are found by imposing equilibrium conditions on Eqs. (2) and (3), yielding

$$P_\ell = E_\ell[s(\alpha)] + \Delta w(\alpha) \frac{\tau}{\alpha}, \quad (13)$$

$$P_o = e_o - \Delta w(\alpha) \frac{\tau}{1 - \alpha}. \quad (14)$$

Note that $s(\alpha)$ and $\Delta w(\alpha)$ are implicit functions of the land fraction but that we lack analytical expressions for them. As α increases in Fig. 6, P_ℓ decreases more strongly than P_o because land precipitation is not only affected by (initially sharply) decreasing $1/\alpha$ but in addition by a reduction in evapotranspiration as s declines. In contrast, ocean precipitation is only reduced by (initially weakly) increasing advection. The additional influence of α on P_ℓ through E_ℓ causes the asymmetry of the $\chi(\alpha)$ mean in Fig. 5b with a minimum around $\alpha = 0.75$ instead of 0.5. Although $\chi(\alpha)$ is expected to be u shaped for every combination of the other parameter values, the exact location of the minimum will differ. Generally, the width of the spread of χ values indicates that the land fraction is the dominant predictor for χ near its extreme values but that its influence weakens toward intermediate values.

With the understanding of the influence of α developed in this section, we can now explain the first two seemingly unphysical behaviors in Fig. 3, as described at the end of section 4. They concern the fact that there is hardly any rain over the ocean when the soil is dry and that ocean advection tends to decrease with increasing s while land advection increases. The model runs which populate the regime of low soil moisture in Fig. 3 share the property of large land fractions and therefore equilibrate to overall dry conditions, both over land and over ocean. Both atmospheres can consequently only yield very little rain. The amount of moisture exchanged between land and ocean translates to an advection rate per unit area that is

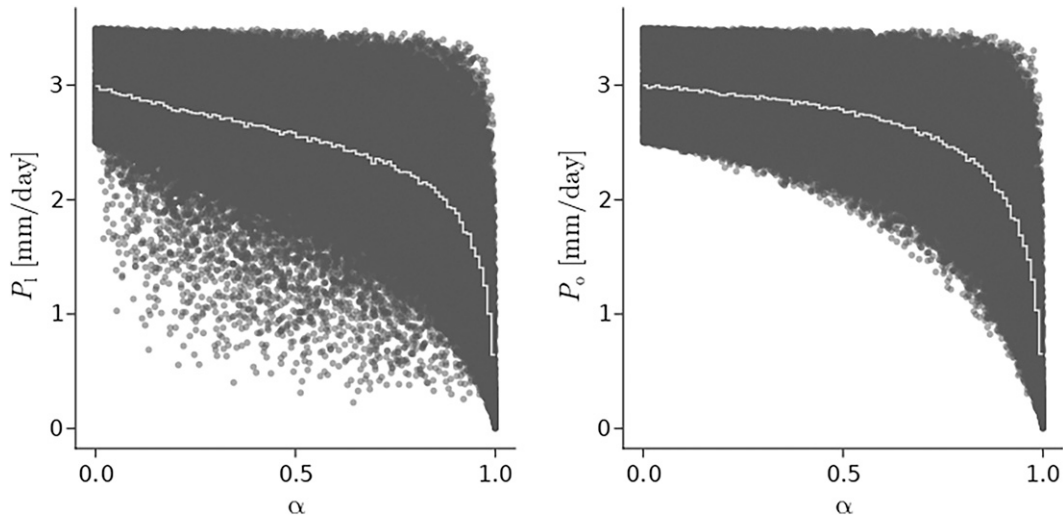


FIG. 6. Ocean precipitation rate P_o and land precipitation rate P_l vs land fraction α . The white lines show χ mean values computed for 100 bins along the α axis. The transition from an ocean-only to a land-only model scenario is marked by a decrease of both precipitation fluxes, indicating overall moist conditions for small land fractions and dry conditions for large land fractions.

high for the small ocean and low for the large land. The opposite situation is found at the largest s values in Fig. 3, which originate from model runs with very small α . There, A_l is at its maximum while A_o nearly vanishes. In the intermediate s -regime, values of α are intermediate and have little influence on the shape of the fluxes.

c. Permanent wilting point s_{pwp} and field capacity s_{fc}

Variations in the soil parameters lead to mean variations of χ similar to the effects of land fraction changes, with the mean varying between $\chi = 0.88$ and 0.98 for both the permanent wilting point (Fig. 5c) and the runoff exponent (Fig. 5d). In Fig. 5c, χ shows an almost linear decrease for an increase in s_{pwp} . To understand this behavior, another thought experiment is helpful: Let us consider a system in equilibrium for some value of the permanent wilting point, e.g., $s_{pwp} = 0.3$, and examine how the system would respond if this value was suddenly changed to $s_{pwp} = 0.4$, as illustrated in Fig. 7. The presented arguments assume that the other parameter values stay fixed when varying s_{pwp} but we can see from the right panel of Fig. 7 that the influence of the permanent wilting point also leaves its imprint on the mean soil moisture state (white line) in the form of a clear increase with s_{pwp} . We therefore make use of the mean value for illustration purposes. The left panel of Fig. 7 depicts the evapotranspiration curves for $s_{pwp} = 0.3$ and 0.4 , respectively, with fixed $e_p = 5.0 \text{ mm day}^{-1}$. Because s_{pwp} and s_{fc} are equidistant for different soil types, a change of s_{pwp} merely shifts the evapotranspiration curve along s .

The mean soil moisture value in the CM data for $s_{pwp} = 0.3$ is $s = 0.45$. This initial state for our thought experiment and its corresponding evapotranspiration value are displayed as blue dots in Fig. 7. An abrupt increase of the permanent wilting point to $s_{pwp} = 0.4$ would lead to the following sequence

of events. First, evapotranspiration experiences an instantaneous drop ΔE_{inst} (first red arrow connecting the blue and green dots). The green dot represents a temporary state where the model is not in equilibrium because the soil receives more moisture from precipitation than it loses through evapotranspiration and runoff. Consequently, the soil moistens. As time progresses, the system attains a new equilibrium state (orange dot) at a higher s value. However, as the soil moistens, not only evapotranspiration but also runoff increases so that the soil does not moisten enough to reach the initial E_l flux. As a consequence, the land atmosphere becomes drier and land advection increases. Since the ocean atmosphere needs to supply more moisture to the land, w_o decreases. Therefore, the increase in advection from increased Δw , needed to balance the increased runoff, is only possible if w_l decreases more strongly than w_o . Accordingly, P_l decreases more strongly than P_o , which explains why χ declines with increasing s_{pwp} .

In effect, the new equilibrium for a larger s_{pwp} value would be characterized by a moister soil with larger runoff but reduced precipitation, thus leaving less moisture to evapotranspiration. The new E_l would be ΔE_{eq} smaller than its initial value. This response to an increase in s_{pwp} is also responsible for the third seemingly unphysical behavior, namely, the decline of evapotranspiration for intermediate s values previously seen in Fig. 3. Precipitation and evapotranspiration are reduced because states with moister soils correspond to simulations with larger s_{pwp} .

d. Runoff exponent r

The relationship between χ and r in Fig. 5d resembles $\chi(s_{pwp})$ but with opposite trend: χ increases with r while it decreases with s_{pwp} . Indeed, the similarity originates from a similar physical mechanism. In the formulation of the runoff

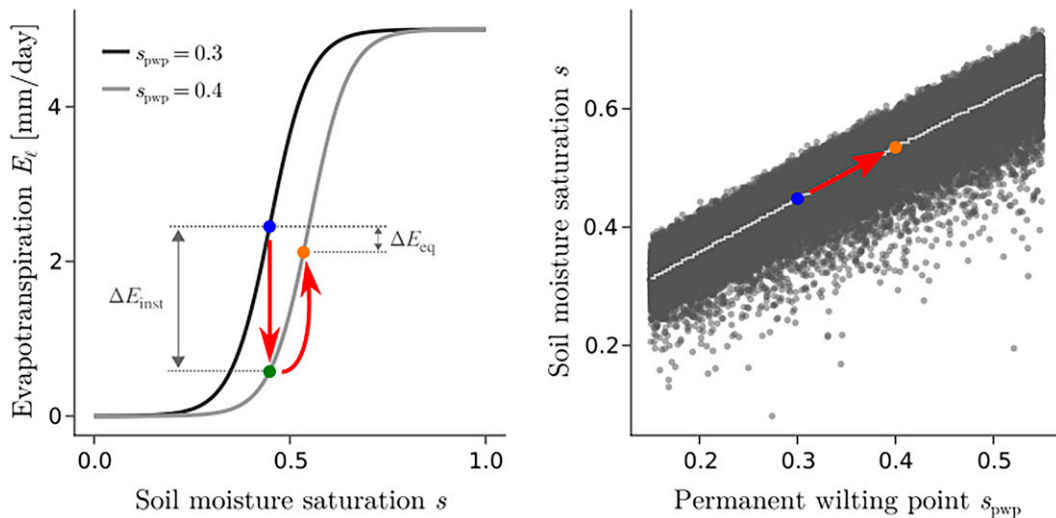


FIG. 7. Influence of an increase in s_{pwp} on the equilibrium state. (left) Higher values of s_{pwp} shift the graph of the E_{ℓ} parameterization toward larger s . (right) Equilibrium values of the soil moisture saturation from CM data plotted against s_{pwp} values. The blue dots mark the initial equilibrium state, the green dot represents a temporary state of soil moisture imbalance due to a sudden increase of s_{pwp} , and the orange dot marks the eventually attained equilibrium state for the new s_{pwp} value.

fraction, $R_f = \epsilon s^r$, r enters as the exponent. As for the s_{pwp} dependence, we can conduct a thought experiment, starting from a system in equilibrium which then responds to a sudden increase of r . Since s has values between zero and one, an increase of the runoff exponent reduces the value of R_f and soil moisture increases. As a consequence, also both atmospheres start to moisten: First, w_{ℓ} increases through increased evapotranspiration from the wetter soil, thereby reducing the moisture difference between land and ocean. Second, the reduction of Δw implies reduced advection with the effect that the ocean atmosphere retains more of its moisture and w_o increases. Eventually, the decreasing advection matches the runoff which started to intensify again after the initial drop. A new equilibrium is attained in which runoff is reduced compared to the initial state with lower r value. Equally reduced land advection with lower Δw reflects more similar atmospheric moisture conditions and, hence, increased χ .

Equilibrium states with higher r value also have stronger precipitation rates from higher w_{ℓ} and w_o . In Fig. 3, we see the influence of r in both the low and high soil moisture regime, where it works in tandem with the land fraction to shape the moisture fluxes. Both precipitation increases for low and high s , respectively, correspond to a combination of increasing r and decreasing α . In these regimes, the combined influence of r and α dominates over the influence of s_{pwp} discussed earlier.

6. Under which circumstances can χ become larger than 1?

So far, we concluded that χ is bounded by an upper limit of one due to the necessity of a net moisture transport from ocean to land and the assumption that the efficiency with

which atmospheric moisture is turned into precipitation is the same over land and ocean. However, we know of local systems in the real world for which higher rain rates are observed over land compared to the adjacent ocean. For instance, Qian (2008), Sobel et al. (2011), Cronin et al. (2015), Wang and Sobel (2017), and Ulrich and Bellon (2019) found precipitation enhancement over tropical islands and attributed this observation mainly to the development of sea breezes triggering precipitating convection over the islands. Even for the full tropics, some observations suggest a χ value slightly larger than one (Hohenegger and Stevens 2022). By construction, our simple model cannot yield χ values larger than one which can be interpreted as a tendency to underestimate real precipitation ratios. In the following, we explore different ways in which our model framework could be modified to enable precipitation enhancement over land, i.e., $\chi > 1$.

a. Relaxing assumptions of the closed model

To begin with, we started out with the hypothesis that precipitation is neither favored by land, nor ocean, meaning that different surface characteristics do not affect the way it rains: for the same water vapor path, the model computes the same amount of rain over land and ocean. In reality, while we can generally expect a moister atmosphere to yield more rainfall, the shape of $P(w)$, determined by the values for the a and b parameters, could differ over different surfaces. With its tendency for too low χ values, our model suggests that our initial hypothesis about $P(w)$ was wrong and that in reality, precipitation is actually favored over land. In the model, we can favor precipitation over land most easily by choosing a smaller b parameter over land than over ocean, leading to higher precipitation rates over land than over ocean for the same water vapor path. As a proof of concept, we ran model simulations

with different choices for b over land and ocean. When choosing b just 0.1% smaller over land than over ocean, already about 20% of the simulations yielded a χ value larger than one. That it rains differently over land and ocean would be in line with the conclusions of Hohenegger and Stevens (2022), who found more precipitation over tropical land than what is expected based on the tropical land–sea distribution and rainbelt position, and also with the results of Ahmed and Schumacher (2017), who found distinct differences in the $P(w)$ relationships over land and ocean based on observations. Further studies examining differences in $P(w)$ over different surface types, and constraining the realistic ranges of the a and b parameters are needed to conclude whether precipitation processes are responsible for the higher χ values found in nature.

Second, we treat all model boxes as being homogeneous and well-mixed which allows us to work with mean fluxes rather than resolving the horizontal direction explicitly. It is well known, however, that an airstream traversing an oceanic region will moisten along its trajectory since mean ocean evaporation typically exceeds mean ocean precipitation and the reverse applies to land regions. Furthermore, Ogino et al. (2016) and Ogino et al. (2017) found that the conventional view in which Earth’s surface gets divided into ocean and land misses out on particular interactions driven by the land–sea contrast which are confined to a coastal region, a few hundred kilometers seaward and landward from the coast. These coastal regions receive more rain than both the open ocean and inland continental regions. Also, Bergemann and Jakob (2016) found that tropical rainfall over land associated with coastal effects such as sea breezes can occur under drier atmospheric conditions than rainfall over the open ocean. Hence, adding coastal zones with a specific coastal precipitation parameterization to the model is another flavor of the argument that—for precipitation enhancement over land—it has to rain differently in different subdomains. Coastal zones might also capture the fact that precipitation enhancement is particularly strong over relatively small landmasses where coastal effects are expected to be more influential.

Third, the model has neither an energy budget, nor a diurnal cycle. As a consequence, phenomena associated with pressure gradient forcing like diurnal sea breezes which tend to enhance precipitation over land are not captured. Energy dependence and a diurnal cycle can be implemented in different ways—either fundamentally by coupling water balance and energy balance equations, or indirectly by introducing a diurnal cycle in energy-dependent parameters such as τ , e_p , or w_{sat} . Even with the same $P(w)$ relationship across the domain, a diurnal cycle may lead to $\chi > 1$ through two pathways: evapotranspiration might be enhanced more strongly than ocean evaporation during the day. At the same time, the wind field would become variable and might exhibit convergence over land, potentially leading to upgradient moisture transport which was formerly disabled due to the assumption of a constant background wind speed. The combined effect of these two pathways may lead to a high enough concentration of moisture over land during the day to yield higher temporary rain rates over land than over ocean. If the reverse transport during the night does not fully compensate for the

daytime precipitation signal, then χ might be larger than one on average. In other words, the diurnal cycle of available energy may explain why χ is close to one and can even be larger than one in reality.

Last, our model configuration with one land and one ocean box is not representative of the real tropics. It is likely that a different land distribution with more boxes would lead to higher χ values because smaller box sizes generally increase the advection efficiencies. If, in addition, the boxes were differently sized, we might see instances where $\chi > 1$. In equilibrium, each ocean atmosphere would still be moister than the leeward land atmosphere, but it cannot be precluded that weighting the precipitation rates by the different box sizes would yield a stronger mean land than ocean precipitation.

b. Opening the closed model

The previous arguments still treat the land–ocean–atmosphere system as a closed model. This assumption may be valid over the full tropics, assuming a negligible net moisture exchange with the extratropics, but it is certainly invalid over islands, where land precipitation enhancement is typically observed. Hence, allowing for atmospheric inflow and outflow out of the domain might create χ values larger than one. We test this hypothesis in two ways.

First, moisture import or export from an external environment outside the model boundaries can be incorporated by an additional advection term, A_{ext} (mm day^{−1}) in Eq. (3) for oceanic water vapor. A positive A_{ext} denotes inflow of external moisture, while a negative A_{ext} means that the ocean atmosphere loses moisture through the model boundaries. This construction mimics the case of an island surrounded by an ocean under the influence of large-scale convergence or divergence. But is this change in the model framework sufficient to create scenarios for which $\chi > 1$?

We argue that the answer is no: regardless of whether the system is gaining or losing moisture through its boundaries, an equilibrium state still requires a net transport of moisture from ocean to land, and therefore $w_o > w_\ell$ with $\chi < 1$. The term A_{ext} acts in a similar fashion as ocean evaporation. Under the influence of moisture convergence, the positive A_{ext} is equivalent to an increase in E_o and merely increases the moisture content in all boxes. In the case of moisture divergence, negative A_{ext} acts like a reduction of E_o and an overall drier equilibrium state is attained as long as $|A_{\text{ext}}| < E_o$. If the loss through the model boundary is stronger than the moisture input from the ocean surface, the system will undergo drying until the trivial solution $\{w_o = 0, w_\ell = 0, s = 0\}$ is reached.

Second, we can also open the model by allowing moisture to enter the domain from one side and leave it on the other side. As an illustrative example for this type of open model, we consider the simplest configuration with a land box of length L_ℓ , placed between two equally big ocean boxes of lengths $L_{o1} = L_{o2}$. The subscript $o1$ refers to the ocean in front of the island as seen by the airflow horizontally traversing the domain at constant wind speed, while $o2$ refers to the ocean behind the island. The equations governing the evolution of

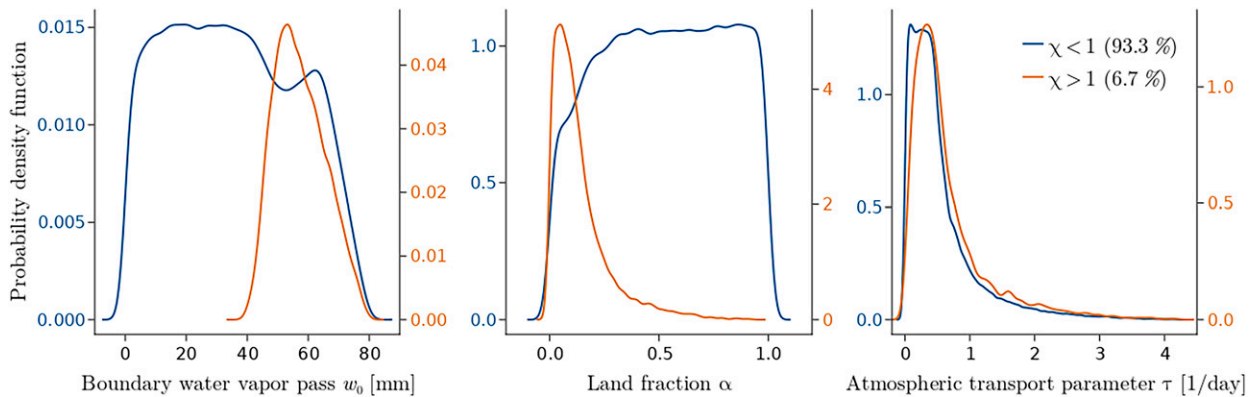


FIG. 8. Probability density functions of parameter values for w_0 , α , and τ . Blue and orange graphs contain data from simulations with χ values smaller and larger than one, respectively. Ratios larger than one are only found for 6.7% of all simulations.

w_{o1} , w_ℓ , and w_{o2} and s are formulated in analogy to the closed model equations and can be found in the [appendix](#) along with a model sketch. This open model requires one additional parameter, the boundary water vapor path w_0 with values between 0 mm and w_{sat} , which denotes the water vapor path at the windward model boundary. It enters the model equations in the advection term for the first ocean. As for the closed model, we perform 100 000 simulations with randomly chosen combinations of parameter values from [Table 1](#) with the modification that the full domain length is varied between 200 and 2000 km. The obtained set of equilibrium solutions is referred to as “OM data.”

In the open model, χ is computed from mean precipitation rates \bar{P}_ℓ and \bar{P}_o as

$$\chi = \frac{\bar{P}_\ell}{\bar{P}_o} = \frac{2P_\ell}{P_{o1} + P_{o2}}. \quad (15)$$

As in the case of the closed model, equilibrium can only be attained if the land atmosphere receives advected moisture from the ocean. In the open model, this means that the first ocean atmosphere has to be moister than the land atmosphere which—sticking to the assumption of the same parameterization for precipitation across the domain—implies $P_{o1} > P_\ell$. It follows from Eq. (15) that a χ value larger than one is possible if the inequality, $P_{o2} < 2P_\ell - P_{o1}$, is fulfilled. This means, the second ocean atmosphere must be dry enough to compensate for the relatively moist first ocean atmosphere, such that the mean ocean precipitation is smaller than P_ℓ . From the OM data, we find that only about 6.7% of all simulations meet this condition and yield $\chi > 1$. As expected, these simulations have in common that atmospheric moisture reduces along the wind trajectory, i.e., $w_0 > w_{o1} > w_\ell > w_{o2}$.

We perform the same sensitivity analysis as for the closed model to understand which parameter combinations lead to χ values larger than one, and to which parameters χ is most sensitive. Opening the model does not fundamentally change the principal sensitivities but modifies their order of importance: The most sensitive parameter is now w_0 with $I_{\text{MI}}(\chi, w_0) = 254$, followed by α with $I_{\text{MI}}(\chi, \alpha) = 202$ and τ with $I_{\text{MI}}(\chi, \tau) = 147$.

All other parameters, including the formerly relevant soil parameters, have I_{MI} values lower than 8 and can be neglected as predictors for χ . To understand which parameter combinations lead to $\chi > 1$, [Fig. 8](#) shows PDFs of the values of w_0 , α , and τ for simulations with χ values smaller and larger than one in blue and orange, respectively. Even though the distributions have a significant overlap, $\chi > 1$ requires a large enough boundary water vapor path $w_0 \geq 38$ mm and becomes more likely with smaller land fractions. States with $\chi > 1$ do not exist for $\alpha > 0.93$ and are most likely around $\alpha = 0.05$. In contrast, a value of $\chi < 1$ seems to be possible with any value for α . Further inspection of the state variable values (not shown) reveals that equilibrium states with $\chi > 1$ are overall moist. Soil moisture saturation values cluster close to and beyond the field capacity. Water vapor path values peak around 48 mm over both land and ocean and never get smaller than 38 mm. Simulations with $\chi < 1$, in contrast, exhibit equilibrium states across the entire moisture spectrum, including very dry states with soil moisture values below the permanent wilting point.

As in the case of the closed model, the open model results are subject to the choice of the land distribution and may change for different numbers of land boxes. In addition, the open model is sensitive to the location of the land box which affects the relative size of the two ocean boxes. However, a test of different asymmetric configurations indicates that the presented statements are only affected quantitatively, not qualitatively.

7. Conclusions

This study was motivated by our lack of theoretical understanding of how tropical precipitation gets partitioned between land and ocean. To provide such understanding, we studied constraints and sensitivities of the precipitation ratio χ , quantifying the ratio between spatiotemporally averaged land and ocean precipitation rates, $\chi = P_\ell/P_o$. Estimates of χ from different observation products range between 0.9 and 1.04 ([Hohenegger and Stevens 2022](#)). We wanted to know how various atmospheric and land processes determine the

value of χ and whether constraints on χ arise from the condition of water mass balance.

We introduced a conceptual box model that describes the rate of change of soil moisture and atmospheric moisture over ocean and land, respectively. The water balance components are expressed by empirical parametric functions of the mean water content of the land and atmospheric boxes. In particular, as a hypothesis, we assumed that precipitation increases exponentially with water vapor path and that the presence of land does not affect this relationship. To investigate the bounds of χ and its parameter sensitivity, we analyzed a large number of equilibrium solutions for different combinations of model parameter values. The obtained results for the case of a closed model with one land and one ocean box can be summarized as follows:

- As long as the land does not affect the relationship between precipitation and water vapor path, χ is bounded by an upper limit of one. This is a direct consequence of the equilibrium condition that the land's loss of water through runoff needs to be compensated for by an equally large net moisture transport from a moister ocean atmosphere to a drier land atmosphere. As precipitation increases exponentially with water vapor path, this necessarily implies stronger precipitation over ocean.
- The lower limit of χ is zero in cases where the land precipitation is zero. Although χ can theoretically vary between zero and one, values between 0.75 and 1.0 appear most likely, with 95% of the simulations falling into this range.
- The free model parameters are listed in Table 1. We find that χ is most sensitive to a variation of the atmospheric transport parameter τ , followed by the two soil parameters permanent wilting point s_{pwp} and runoff exponent r , and land fraction α . Efficient atmospheric transport for high τ values leads to similar moisture conditions over land and ocean, which results in high χ values. Land fraction is most influential near its extreme values, $\alpha \rightarrow 0$ and $\alpha \rightarrow 1$, where in both cases χ is close to one. Near these extremes, the highly efficient advection rate into or out of the respective tiny land or ocean atmosphere creates similar atmospheric conditions in both boxes. A χ minimum is located at intermediate α values. Finally, χ decreases with increasing permanent wilting point and increases with increasing r . This can be understood from the way in which these parameters control the amount of evapotranspiration (for s_{pwp}) and runoff (for r), and thereby the amount of advective moisture inflow into the land atmosphere required for equilibrium. A larger moisture inflow corresponds to a larger moisture difference between land and ocean atmospheres and, hence, to a lower value of χ .
- The closed water balance model cannot explain observed island precipitation enhancement as reported by other studies because χ is bounded by one. Our interpretation of this finding is that precipitation enhancement over land requires the land to affect the relationship between precipitation and water vapor path, that precipitation enhancement is linked to the presence of a diurnal cycle, that a different land distribution is required, or that it is only possible in an

open model which allows for net advection into or out of the domain. We tested this last option with an open model configuration in which moisture can enter the model through the windward boundary and leave on the other side. For this setup, χ values larger than one exist for a small subset (6.7%) of the performed simulations. These cases require a sufficiently large moisture inflow with a boundary water vapor path of at least $w_0 = 38$ mm, and small land sizes, typically around $\alpha \approx 0.05$ and no larger than $\alpha = 0.93$. The most influential parameters for the open model are w_0 , α , and τ , while the soil parameters are no longer important.

Even though the simple conceptual model does not capture the full range of physical processes that influence the land-sea precipitation contrast in reality, it is able to constrain χ and identifies the efficiency of atmospheric transport as the dominant factor controlling the value of χ . In fact, understanding how advection changes following a change in the model parameter values turned out to be key for understanding how the value of χ changes.

Acknowledgments. We thank Victor Brovkin and the anonymous reviewers for useful comments on the manuscript and George Datseris for fruitful discussions and technical advice.

Data availability statement. The code base used for generating the data and figures for this work is freely available at <https://github.com/Lucalino/OcelandModel>.

APPENDIX

Open Model Formulation

The equations governing an open model configuration with an island (subscript ℓ) between two ocean boxes (subscripts $o1$ and $o2$ in the order of their appearance along the wind trajectory) are similar to the ones for the closed model introduced in section 2 (Fig. A1). However, four instead of three equations are needed,

$$\frac{ds}{dt} = \frac{1}{nz_r} [P(w_\ell) - R(s, w_\ell) - E(s)], \quad (\text{A1})$$

$$\frac{dw_{o1}}{dt} = E_o - P(w_{o1}) + \frac{(w_0 - w_{o1})u}{L_{o1}}, \quad (\text{A2})$$

$$\frac{dw_\ell}{dt} = E(s) - P(w_\ell) + \frac{(w_{o1} - w_\ell)u}{L_\ell}, \quad (\text{A3})$$

$$\frac{dw_{o2}}{dt} = E_o - P(w_{o2}) + \frac{(w_\ell - w_{o2})u}{L_{o2}}. \quad (\text{A4})$$

The lengths of the model subdomains can be written as $L_{o1} = L_{o2} = (1 - \alpha)L/2$ and $L_\ell = \alpha L$, where L denotes the full model domain length.

For a small number of parameter combinations, the algorithm could not determine an equilibrium solution to the open model equations.

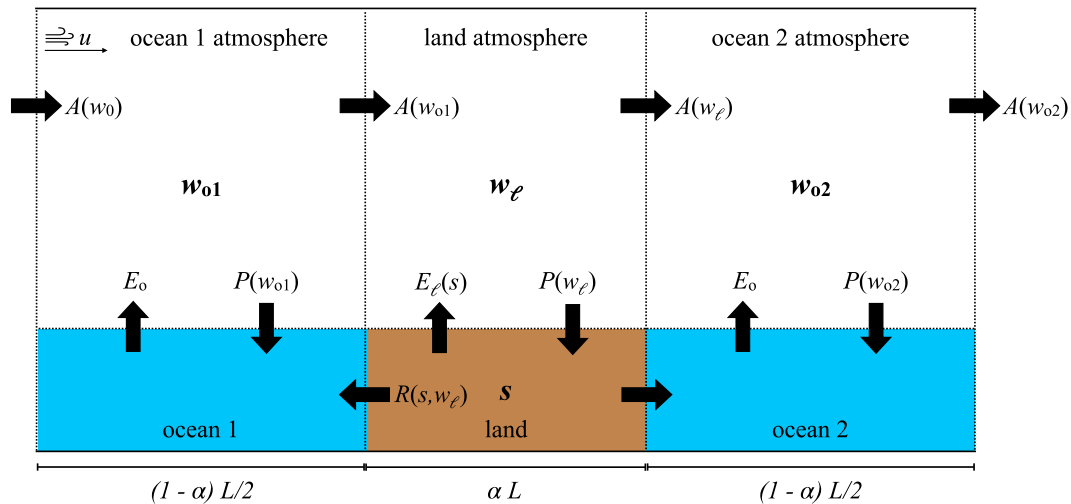


FIG. A1. Sketch of a land–ocean–atmosphere system consisting of an island between two ocean boxes with atmospheric boxes above. The lateral model boundaries are open, allowing moisture to enter and leave the modeled domain. The water vapor path value at the windward model boundary is given by the parameter w_0 and may reflect synoptic-scale atmospheric conditions. Moisture fluxes between boxes are analogous to the closed model described in section 2.

REFERENCES

- Ahmed, F., and C. Schumacher, 2017: Geographical differences in the tropical precipitation–moisture relationship and rain intensity onset. *Geophys. Res. Lett.*, **44**, 1114–1122, <https://doi.org/10.1002/2016GL071980>.
- Bergemann, M., and C. Jakob, 2016: How important is tropospheric humidity for coastal rainfall in the tropics? *Geophys. Res. Lett.*, **43**, 5860–5868, <https://doi.org/10.1002/2016GL069255>.
- Bretherton, C. S., M. E. Peters, and L. E. Back, 2004: Relationships between water vapor path and precipitation over the tropical oceans. *J. Climate*, **17**, 1517–1528, [https://doi.org/10.1175/1520-0442\(2004\)017<1517:RBWVPA>2.0.CO;2](https://doi.org/10.1175/1520-0442(2004)017<1517:RBWVPA>2.0.CO;2).
- Brubaker, K., D. Entekhabi, and P. S. Eagleson, 1991: Atmospheric water vapor transport: Estimation of continental precipitation recycling and parameterization of a simple climate model. NTRS-NASA Tech. Rep. R91-18, 182 pp., <https://ntrs.nasa.gov/api/citations/19910018381/downloads/19910018381.pdf>.
- Brubaker, K. L., D. Entekhabi, and P. S. Eagleson, 1993: Estimation of continental precipitation recycling. *J. Climate*, **6**, 1077–1089, [https://doi.org/10.1175/1520-0442\(1993\)006<1077:EOCPR>2.0.CO;2](https://doi.org/10.1175/1520-0442(1993)006<1077:EOCPR>2.0.CO;2).
- Budyko, M. I., 1956: *Heat Balance of the Earth's Surface*. U.S. Weather Bureau, 259 pp.
- , and O. A. Drozdov, 1953: Characteristics of the moisture circulation in the atmosphere. *Izv. Akad. Nauk SSSR, Ser. Geogr. Geofiz.*, **4**, 5–14.
- Cronin, T. W., K. A. Emanuel, and P. Molnar, 2015: Island precipitation enhancement and the diurnal cycle in radiative-convective equilibrium. *Quart. J. Roy. Meteor. Soc.*, **141**, 1017–1034, <https://doi.org/10.1002/qj.2443>.
- Datseris, G., 2018: DynamicalSystems.jl: A Julia software library for chaos and nonlinear dynamics. *J. Open Source Software*, **3**, 598, <https://doi.org/10.21105/joss.00598>.
- , and U. Parlitz, 2022: *Nonlinear Dynamics*. 1st ed. Springer International Publishing, 236 pp.
- Eltahir, E. B., and R. L. Bras, 1994: Precipitation recycling in the Amazon basin. *Quart. J. Roy. Meteor. Soc.*, **120**, 861–880, <https://doi.org/10.1002/qj.49712051806>.
- Entekhabi, D., I. Rodriguez-Iturbe, and R. L. Bras, 1992: Variability in large-scale water balance with land surface–atmosphere interaction. *J. Climate*, **5**, 798–813, [https://doi.org/10.1175/1520-0442\(1992\)005<0798:VILSWB>2.0.CO;2](https://doi.org/10.1175/1520-0442(1992)005<0798:VILSWB>2.0.CO;2).
- Fiedler, S., and Coauthors, 2020: Simulated tropical precipitation assessed across three major phases of the Coupled Model Intercomparison Project (CMIP). *Mon. Wea. Rev.*, **148**, 3653–3680, <https://doi.org/10.1175/MWR-D-19-0404.1>.
- Hagemann, S., and T. Stacke, 2015: Impact of the soil hydrology scheme on simulated soil moisture memory. *Climate Dyn.*, **44**, 1731–1750, <https://doi.org/10.1007/s00382-014-2221-6>.
- Hohenegger, C., and B. Stevens, 2022: Tropical continents rainier than expected from geometrical constraints. *AGU Adv.*, **3**, e2021AV000636, <https://doi.org/10.1029/2021AV000636>.
- Horton, R. E., 1943: Hydrologic interrelations between lands and oceans. *Eos, Trans. Amer. Geophys. Union*, **24**, 753–764, <https://doi.org/10.1029/TR024i002p00753>.
- Kumar, B. P., M. F. Cronin, S. Joseph, M. Ravichandran, and N. Sureshkumar, 2017: Latent heat flux sensitivity to sea surface temperature: Regional perspectives. *J. Climate*, **30**, 129–143, <https://doi.org/10.1175/JCLI-D-16-0285.1>.
- Lintner, B. R., P. Gentine, K. L. Findell, F. D'Andrea, A. H. Sobel, and G. D. Salvucci, 2013: An idealized prototype for large-scale land–atmosphere coupling. *J. Climate*, **26**, 2379–2389, <https://doi.org/10.1175/JCLI-D-11-00561.1>.
- Masunaga, H., and B. E. Mapes, 2020: A mechanism for the maintenance of sharp tropical margins. *J. Atmos. Sci.*, **77**, 1181–1197, <https://doi.org/10.1175/JAS-D-19-0154.1>.
- Ogino, S.-Y., M. D. Yamanaka, S. Mori, and J. Matsumoto, 2016: How much is the precipitation amount over the tropical coastal region? *J. Climate*, **29**, 1231–1236, <https://doi.org/10.1175/JCLI-D-15-0484.1>.
- , —, —, and —, 2017: Tropical coastal dehydrator in global atmospheric water circulation. *Geophys. Res. Lett.*, **44**, 11 636–11 643, <https://doi.org/10.1002/2017GL075760>.
- Peixóto, J. P., and A. H. Oort, 1983: The atmospheric branch of the hydrological cycle and climate. *Variations in the Global*

- Water Budget*, A. Street-Perrott, M. Beran, and R. Ratcliffe, Eds., Springer, 5–65.
- Qian, J.-H., 2008: Why precipitation is mostly concentrated over islands in the maritime continent. *J. Atmos. Sci.*, **65**, 1428–1441, <https://doi.org/10.1175/2007JAS2422.1>.
- Rodriguez-Iturbe, I., D. Entekhabi, and R. L. Bras, 1991: Nonlinear dynamics of soil moisture at climate scales: 1. Stochastic analysis. *Water Resour. Res.*, **27**, 1899–1906, <https://doi.org/10.1029/91WR01035>.
- Schiro, K. A., J. D. Neelin, D. K. Adams, and B. R. Lintner, 2016: Deep convection and column water vapor over tropical land versus tropical ocean: A comparison between the amazon and the tropical western Pacific. *J. Atmos. Sci.*, **73**, 4043–4063, <https://doi.org/10.1175/JAS-D-16-0119.1>.
- , S. C. Sullivan, Y.-H. Kuo, H. Su, P. Gentine, G. S. Elsaesser, J. H. Jiang, and J. D. Neelin, 2020: Environmental controls on tropical mesoscale convective system precipitation intensity. *J. Atmos. Sci.*, **77**, 4233–4249, <https://doi.org/10.1175/JAS-D-20-0111.1>.
- Seneviratne, S. I., T. Corti, E. L. Davin, M. Hirschi, E. B. Jaeger, I. Lehner, B. Orlowsky, and A. J. Teuling, 2010: Investigating soil moisture–climate interactions in a changing climate: A review. *Earth-Sci. Rev.*, **99**, 125–161, <https://doi.org/10.1016/j.earscirev.2010.02.004>.
- Shannon, C. E., 1948: A mathematical theory of communication. *Bell Syst. Tech. J.*, **27**, 379–423, <https://doi.org/10.1002/j.1538-7305.1948.tb01338.x>.
- Sobel, A. H., and G. Bellon, 2009: The effect of imposed drying on parameterized deep convection. *J. Atmos. Sci.*, **66**, 2085–2096, <https://doi.org/10.1175/2008JAS2926.1>.
- , C. D. Burleyson, and S. E. Yuter, 2011: Rain on small tropical islands. *J. Geophys. Res.*, **116**, D08102, <https://doi.org/10.1029/2010JD014695>.
- Ulrich, M., and G. Bellon, 2019: Superenhancement of precipitation at the center of tropical islands. *Geophys. Res. Lett.*, **46**, 14872–14880, <https://doi.org/10.1029/2019GL084947>.
- van der Ent, R. J., H. H. G. Savenije, B. Schaeffli, and S. C. Steele-Dunne, 2010: Origin and fate of atmospheric moisture over continents. *Water Resour. Res.*, **46**, W09525, <https://doi.org/10.1029/2010WR009127>.
- Wang, S., and A. H. Sobel, 2017: Factors controlling rain on small tropical islands: Diurnal cycle, large-scale wind speed, and topography. *J. Atmos. Sci.*, **74**, 3515–3532, <https://doi.org/10.1175/JAS-D-16-0344.1>.
- Zhang, G. J., and M. J. McPhaden, 1995: The relationship between sea surface temperature and latent heat flux in the equatorial Pacific. *J. Climate*, **8**, 589–605, [https://doi.org/10.1175/1520-0442\(1995\)008<0589:TRBSST>2.0.CO;2](https://doi.org/10.1175/1520-0442(1995)008<0589:TRBSST>2.0.CO;2).